RESEARCH ARTICLE

Key Points:
- Stratospheric aerosol geoengineering intensifies polar vortices
- Circulation effects of stratospheric aerosols not represented by solar dimming
- Effects of sulfate and titania aerosol qualitatively similar

Stratospheric dynamics and midlatitude jets under geoengineering with space mirrors and sulfate and titania aerosols

A. J. Ferraro[1,2], A. J. Charlton-Perez[1], and E. J. Highwood[1]

[1]Department of Meteorology, University of Reading, Reading, UK, [2]College of Engineering, Mathematics and Physical Sciences, University of Exeter, Exeter, UK

Abstract The impact on the dynamics of the stratosphere of three approaches to geoengineering by solar radiation management is investigated using idealized simulations of a global climate model. The approaches are geoengineering with sulfate aerosols, titania aerosols, and reduction in total solar irradiance (representing mirrors placed in space). If it were possible to use stratospheric aerosols to counterbalance the surface warming produced by a quadrupling of atmospheric carbon dioxide concentrations, tropical lower stratospheric radiative heating would drive a thermal wind response which would intensify the stratospheric polar vortices. In the Northern Hemisphere this intensification results in strong dynamical cooling of the polar stratosphere. Northern Hemisphere stratospheric sudden warming events become rare (one and two in 65 years for sulfate and titania, respectively). The intensification of the polar vortices results in a poleward shift of the tropospheric midlatitude jets in winter. The aerosol radiative heating enhances the tropical upwelling in the lower stratosphere, influencing the strength of the Brewer-Dobson circulation. In contrast, solar dimming does not produce heating of the tropical lower stratosphere, and so there is little intensification of the polar vortex and no enhanced tropical upwelling. The dynamical response to titania aerosol is qualitatively similar to the response to sulfate.

1. Introduction

The prospect of intentional manipulation of the Earth's climate, termed geoengineering (or climate engineering), has received some interest in recent years as human emissions of greenhouse gases have continued unabated and climate model projections suggest that global mean surface warming will continue into the 21st century under most emissions scenarios [*Knutti and Sedláček*, 2012]. One approach to geoengineering is to reduce the amount of solar radiation absorbed by the Earth system, an approach called solar radiation management (SRM). This could theoretically be achieved by, for example, placing reflectors at a Lagrange point between the Earth and the Sun [*Angel*, 2006] or adding aerosols to the stratosphere [*Rasch et al.*, 2008]. SRM approaches have received considerable interest because of the potentially large and rapid surface cooling achievable [*Lenton and Vaughan*, 2009]. However, SRM also poses potential risks [*Robock et al.*, 2009]. It is important to quantify the climate response to SRM in order to appropriately characterize these risks.

Climate model studies have shown that, though SRM could potentially be used to reduce global mean temperatures, a perfect compensation of warming induced by greenhouse gases is not possible [*Jones et al.*, 2010; *Kravitz et al.*, 2013]. Potential negative impacts of SRM include global reductions in precipitation [*Bala et al.*, 2008], regionally inhomogeneous impacts [*Robock et al.*, 2008; *Ricke et al.*, 2010; *Irvine et al.*, 2010], and, in the case of SRM with stratospheric aerosols, ozone depletion [*Tilmes et al.*, 2008, 2009].

Much of the research on the impacts of SRM on the stratosphere has focused on ozone chemistry [*Tilmes et al.*, 2008, 2009; *Pitari et al.*, 2014]. However, SRM with stratospheric aerosols would affect the dynamics of the stratosphere even without the effects of ozone changes on stratospheric radiative heating and the consequent dynamical adjustment. The stratospheric polar vortex intensifies in response to the radiative effects of stratospheric sulfate aerosol produced by volcanic eruptions [*Ramachandran et al.*, 2000; *Stenchikov et al.*, 2006], suggesting that a similar response to stratospheric aerosol geoengineering is likely. *Ferraro et al.* [2011] showed that tropical stratospheric radiative heating by geoengineering aerosols increases the meridional temperature gradient in the lower stratosphere. By the principle of thermal wind

balance, the pressure gradient associated with these changes would be expected to produce westerly wind anomalies in the stratosphere. In a simulation of stratospheric sulfate aerosol geoengineering with a chemistry climate model, *Tilmes et al.* [2009] showed intensified stratospheric polar vortices, consistent with the volcanic analog and radiative expectations. The stronger, colder vortices reduced column ozone at high latitudes. This vortex intensification has also been found in model studies of geoengineering with other aerosol types, such as black carbon [*Kravitz et al.*, 2012], which produces very strong radiative heating.

Geoengineering might also affect the stratospheric Brewer-Dobson circulation (BDC), which plays a key role in transporting water vapor and ozone [*Butchart*, 2014], and would also affect the aerosol distribution produced by stratospheric aerosol geoengineering [*Heckendorn et al.*, 2009; *Benduhn and Lawrence*, 2013]. The BDC is projected to strengthen under global warming due to greenhouse gases [*Butchart et al.*, 2011]. This results from increased wave driving of the stratosphere, though there is little change in wave generation at source in the lower troposphere [*Garcia and Randel*, 2008]. *Shepherd and McLandress* [2010] suggest that it is due to the strengthening of the westerlies on the upper flanks of the subtropical jets, which allows more Rossby wave activity to penetrate into the subtropical stratosphere. If geoengineering could counteract the tropospheric warming associated with greenhouse gas increases, it should also counteract the intensification of the upper flanks of the subtropical jets. However, the wind changes in the stratosphere associated with aerosol radiative heating could also influence the wave driving of the BDC. *Niemeier et al.* [2011] show that the radiative heating in the lower stratosphere from the geoengineering aerosol enhances the tropical upwelling of the BDC, increasing aerosol lifetime in the stratosphere. *Aquila et al.* [2014] show that this also slows the downward propagation of the Quasi-Biennial Oscillation. This study will compare the response of the BDC to geoengineering and increasing carbon dioxide concentrations.

In addition to the relevance of stratospheric temperature and circulation for column ozone levels, the stratosphere has been shown to exert an influence on the midlatitude tropospheric circulation on a range of time scales. *Baldwin and Dunkerton* [1999, 2001] showed that stratospheric polar vortex anomalies associated with planetary wave variability can propagate downward into the troposphere on time scales of a week, where they persist for up to 2 months. A strengthened polar vortex tends to produce a poleward shift in the eddy-driven tropospheric jet. Thus, the stratospheric response to geoengineering could be important in predicting and understanding the tropospheric response.

In this study the response of the dynamics of the stratosphere to SRM geoengineering and the potential influence on the troposphere will be investigated using a global climate model. The following potential SRM implementations will be investigated: space reflectors, sulfate aerosol, and titania aerosol. Geoengineering using space reflectors can be represented in climate models by a reduction in total solar irradiance. Such solar dimming experiments are included in the SRM simulations of the Geoengineering Model Intercomparison Project (GeoMIP) [*Kravitz et al.*, 2011]. Solar dimming would produce a rather different stratospheric response to aerosols, since it does not represent their local radiative effects [*Ammann et al.*, 2010; *Niemeier et al.*, 2013]. We therefore contrast the solar dimming experiment with the two aerosol SRM experiments. Though sulfate was initially proposed for geoengineering in analog with the climatic effects of volcanic eruptions [*Budyko*, 1977], other aerosols, such as titanium dioxide (titania), may prove more suitable because of their greater scattering efficiencies for solar radiation and reduced stratospheric heating [*Ferraro et al.*, 2011] or reduced ozone depletion [*Pope et al.*, 2012]. Therefore, titania aerosol is also investigated in this study because of its strong scattering properties.

2. Climate Model Simulations

The University of Reading Intermediate General Circulation Model (IGCM) [*Forster et al.*, 2000] is used in this study. It is a spectral model which uses triangular truncation of spherical harmonics at wave number 42 (T42; corresponding to a horizontal resolution of approximately 2.7°) and has 35 levels with the model top at 0.1 hPa. It uses the *Morcrette* [1991] radiation scheme to calculate diurnally averaged radiative fluxes. It has previously been used in a very similar configuration to study the downward propagation of the stratospheric dynamical response to fluctuations in solar irradiance [*Cnossen et al.*, 2011].

The model has a simple gravity wave drag parameterization scheme, described by *Cnossen et al.* [2011]. Some Rayleigh friction is included above 1 hPa to prevent spurious wave reflections from the model top. Stratospheric ozone concentrations are fixed using the monthly climatology of *Li and Shine* [1995]. This model configuration does not include interactive ozone chemistry and consequently cannot represent

Table 1. Summary of Climate Model Simulations

Name	CO$_2$ Concentration (ppmv)	Geoengineering	Global Mean Surface Temperature Change (K)
Control	355	–	0
4CO$_2$	1420	–	4.20
4CO$_2$ + *Sulfate*	1420	Sulfate aerosol	−0.28
4CO$_2$ + *Solar*	1420	3.4% reduction in total solar irradiance	0.10
4CO$_2$ + *Titania*	1420	Titania aerosol	−0.12

the dynamical response to changing ozone concentrations. This is an important limitation since sulfate aerosol geoengineering is expected to strongly impact stratospheric ozone concentrations [*Tilmes et al.*, 2008, 2009; *Pitari et al.*, 2014]. Potential interactions between ozone concentrations and the dynamics of the stratosphere are discussed in section 4.

The model includes a mixed-layer "slab" ocean 100 m in depth. Ocean heat fluxes are calculated from the surface energy imbalance diagnosed when the model is integrated with sea surface temperatures fixed according to the ERA-40 reanalysis [*Uppala et al.*, 2005].

Bell et al. [2009] show that the IGCM simulates similar stratospheric variability to reanalysis data. *Ferraro* [2013, chap. 3] provides a detailed description of the model as used here and compares stratospheric and tropospheric climate with reanalysis data and other observational data sets. They find its representation of mean climate to be similar to many current climate models, including those in the Coupled Model Intercomparison Project Phase 5 (CMIP5) archive. The IGCM's main deficiencies are similar to those in other climate models. For example, subtropical stratocumulus cover is too low [*Nam et al.*, 2012], and too many stratospheric sudden warming events occur late in Northern Hemisphere winter [*Charlton-Perez et al.*, 2013]. It simulates a poleward shift of the midlatitude jets in response to increasing carbon dioxide concentrations, a robust result among climate models [*Yin*, 2005; *Lorenz and DeWeaver*, 2007; *Lu et al.*, 2008].

Equilibrium climate model simulations (summarized in Table 1) 80 years in length are used. Since the model has a slab ocean, it equilibrates to the perturbations applied here within 15 years, so the final 65 years of each simulation is used for equilibrium analysis. The climate model simulations of geoengineering are compared with a *Control* climate with twentieth century carbon dioxide (CO$_2$) concentrations and a simulation in which the carbon dioxide concentrations are instantaneously quadrupled (4CO$_2$).

Three potential implementations of SRM geoengineering to counterbalance the surface warming from a quadrupling of CO$_2$ are investigated. This is a substantial perturbation to the planetary radiation budget, chosen so the responses and their physical mechanisms can be clearly identified rather than for realism. It has been suggested that geoengineering may be deployed more subtly [e.g., *Keith et al.*, 2010].

The 4CO$_2$+*Solar* simulation reduces total solar irradiance, representing geoengineering using space mirrors. This simulation is similar to the GeoMIP *G1* experimental design [*Kravitz et al.*, 2011] (though *G1* uses the preindustrial climate as the control, whereas here we use the present-day climate). The 4CO$_2$+*Sulfate* and 4CO$_2$+*Titania* simulations represent stratospheric aerosol geoengineering with either sulfate or titania aerosol. We assume that geoengineering is deployed in such a way as to produce a permanent stratospheric aerosol layer, with an injection rate matching the rate at which aerosol is removed from the stratosphere. We therefore prescribe a time-invariant zonal mean aerosol spatial distribution. There is some uncertainty over the latitudinal distribution of aerosols that would result from continuous aerosol injection in the tropical stratosphere, with some models producing a relatively uniform layer and others with a concentration strongly peaked in the tropics [*Pitari et al.*, 2014]. We choose a distribution which mimics the results of simulations of tropical sulfur injection in aerosol microphysical models [*Heckendorn et al.*, 2009; *Niemeier et al.*, 2011], similar to a recently proposed standard prescribed distribution for chemistry climate model studies [*Tilmes et al.*, 2014]. Two key features of these distributions are a peak in aerosol mass mixing ratio at the injection point and an aerosol layer at higher altitude in the tropics than at the poles due to the overturning of the Brewer-Dobson circulation. The distribution is shown in Figure 1 and described further in Text S1 in the supporting information. The aerosol concentration is changed in the same proportion everywhere, so the aerosol mass burden balances the surface warming from a quadrupling of CO$_2$. The shape
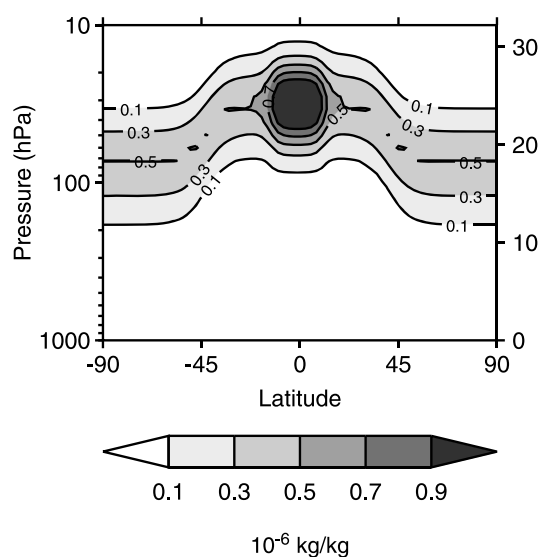
Figure 1. Zonal mean sulfate aerosol mass mixing ratio in units of 10^{-6} kg/kg.

of the distribution is the same for titania aerosol, but the required aerosol burden is lower since titania is a more efficient scatterer of solar radiation because of its high refractive index at solar wavelengths [*Ferraro et al.*, 2011].

Aerosol optical properties are calculated assuming spherical particles with a lognormal distribution with median radius of 0.1 μm and a geometric standard deviation of 2.0. Sulfate aerosol refractive indices are from *World Meteorological Organisation* [1986], and titania aerosol refractive indices are from *Ribarsky* [1985]. Refractive indices for sulfate and titania are provided in the supporting information (Data Sets S1 and S2) and presented in Figure S1. It is likely that, at the injection rates required to maintain a stratospheric aerosol loading capable of counteracting the surface warming from a quadrupling of CO_2, coagulation processes would result in a larger median radius and increased gravitational settling such that such a large radiative forcing may not be possible [*Heckendorn et al.*, 2009; *English et al.*, 2012], so our choices should not be interpreted as realistic predictions. However, since stratospheric aerosol geoengineering is an imagined technology, we do not yet know what technologies or injection strategies may be available which may help reduce coagulation (for example, direct injection of sulfuric acid gas rather than sulfur dioxide, as described by *Pierce et al.* [2010]; though smaller aerosols would decrease stratospheric ozone more than larger ones, as shown by *Tilmes et al.* [2008]). Consequently, we describe the general aspects and physical mechanisms of the stratospheric response in this paper while discussing the potential effects of uncertainties in the aerosol size and spatial distribution in section 4.

3. Results

3.1. Zonal Mean Temperature and Zonal Wind

We begin by investigating the changes in zonal mean zonal winds and temperatures in response to stratospheric aerosol geoengineering. Zonal mean responses are presented for the solsticial seasons when there is a polar vortex in the winter hemisphere.

The zonal mean temperature response to geoengineering is presented as the difference between the geoengineering and $4CO_2$ simulations (Figure 2) in order to emphasize the effect of the aerosol rather than the substantial stratospheric cooling from the increased CO_2 concentrations. Corresponding differences relative to the *Control* simulation are shown in Figure S2. In the geoengineering simulations the troposphere, as expected, cools relative to $4CO_2$ (see zonal mean changes in Figure 2 and surface temperature changes in Figure S3). The stratosphere, however, exhibits a range of responses depending on the interplay between radiative heating and cooling and the dynamical response to these radiative changes. In their radiative calculations with fixed dynamics, *Ferraro et al.* [2011] showed that sulfate produces a stronger tropical lower stratospheric heating than titania due to greater absorption of longwave radiation. However, in these general circulation model simulations, titania produces stronger tropical warming than sulfate. Differences cannot be unambiguously attributed to the dynamical response because the climate model used here has a different radiation code (that of *Morcrette* [1991]) from that used by *Ferraro et al.* [2011] (that of *Edwards and Slingo* [1996]). However, this feature could be explained by different effects of the aerosols on the upwelling branch of the Brewer-Dobson circulation (discussed in section 3.4). The warming of the summer polar stratosphere by titania (Figures 2e and 2f) is a result of shortwave absorption, which is stronger for titania than it is for sulfate (Figure S1).

Ferraro et al. [2011] showed that sulfate has little radiative effect on the temperature of the winter polar stratosphere. However, the temperature response to sulfate in these climate model simulations, where the circulation is allowed to respond, shows Northern Hemisphere (NH) polar stratospheric cooling of up to 16 K
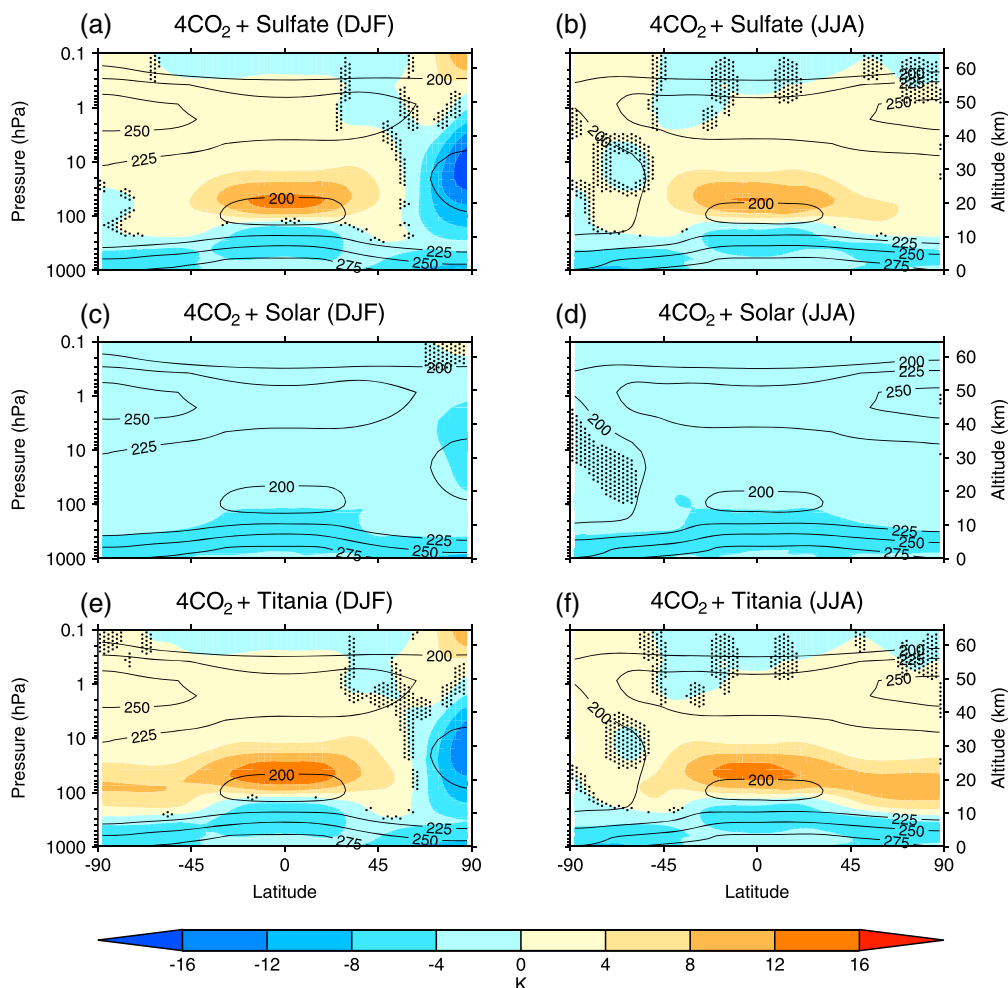
Figure 2. Zonal mean temperature difference between geoengineering and $4CO_2$ simulations. Differences are taken between the mean of the final 65 years of the $4CO_2$ and the geoengineering simulations. The $4CO_2$ climatology (K) is shown by the contours. Stippling shows regions where the response is not statistically significant at the 95% level using a Student's t test.

(Figures 2a and 2e). This suggests a dynamical feedback associated with a strengthened Arctic polar vortex, which acts to isolate the polar stratosphere, allowing radiative cooling to dominate. A similar response is seen for titania. The characteristics of the polar vortex response will be investigated further below.

We compare the zonal mean zonal wind response to the combination of geoengineering and increased CO_2 with the $4CO_2$ simulation in Figure 3, again to emphasize the effects of the aerosol rather than that part of the response resulting from the increased CO_2 concentrations. Corresponding differences relative to the *Control* simulation are shown in Figure S4. Figure S4 also shows the model's response in the $4CO_2$ simulation relative to *Control*. In Northern Hemisphere (NH) winter (December-January-February; DJF) $4CO_2$ produces midlatitude stratospheric westerly anomalies of 4–8 m s^{-1} between around 100 and 5 hPa. In the NH upper stratosphere there is an easterly anomaly which is a consequence of increased drag from the planetary wave breaking (shown by the increased upper stratospheric Eliassen-Palm flux convergence in Figure S5). The weakening of the polar vortex above 5 hPa due to increasing wave drag in $4CO_2$ is consistent with the results of *Rind et al.* [1998] and *Bell et al.* [2010]. *Manzini et al.* [2014] showed that CMIP5 models predict a weakening of the polar vortex in response to increasing CO_2 at lower altitudes (below 10 hPa) as well. This feature is only seen in 66% of the models considered in that study, indicating that there is still some uncertainty on the sign of zonal wind changes in the Arctic stratosphere in response to increasing CO_2 concentrations. The intermodel disagreement on the response to increasing CO_2 concentrations
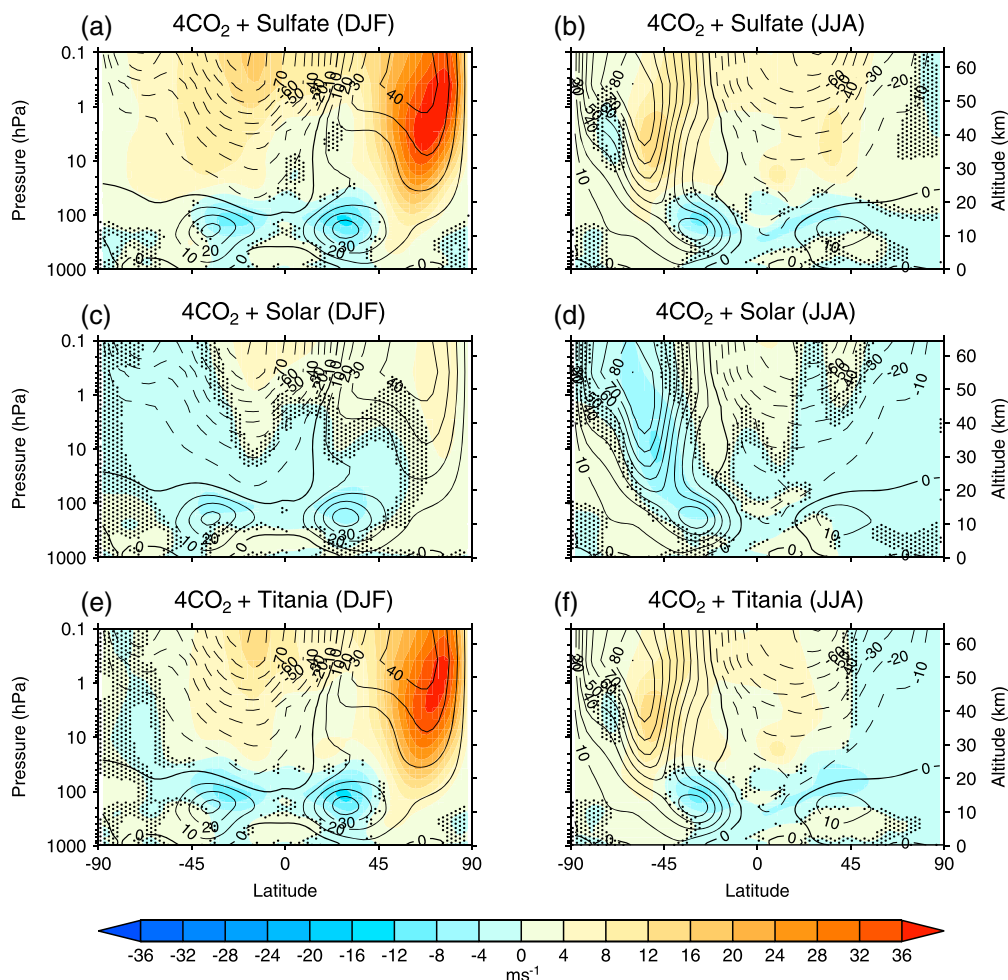
Figure 3. Zonal mean zonal wind difference between geoengineering and $4CO_2$ simulations. Differences are taken between the mean of the final 65 years of the control and the $4CO_2$ and geoengineering simulations. The $4CO_2$ climatology (m s^{-1}) is shown by the contours. Stippling shows regions where the response is not statistically significant at the 95% level using a Student's t test.

calls into question the reliability of model results of the stratospheric response to geoengineering and CO_2 together, especially when only one model is considered as is done here. There are also westerly anomalies on the upper flanks of the subtropical jets, in thermal wind balance with the tropospheric warming and stratospheric cooling in response to increasing CO_2 concentrations. This response increases the meridional temperature gradient in the lower stratosphere and drives westerly wind anomalies aloft.

It was hypothesized in section 1 that, as a consequence of tropical lower stratospheric warming, geoengineering aerosols would drive a westerly wind anomaly in the midlatitude to high-latitude stratosphere. In winter this response corresponds to an intensification of the stratospheric polar vortex.

Our climate model simulations show that this does indeed happen. In NH winter, sulfate aerosol geoengineering approximately doubles the strength of the mean winds in the lower part of the NH polar vortex (Figure 3a). For titania (Figure 3e) the response is qualitatively similar to sulfate but smaller in magnitude since the smaller mass of titania has less of an effect on the meridional temperature gradient. There are also statistically significant wind anomalies in the troposphere, suggestive of a shift in the tropospheric jets. The latitude of the midlatitude eddy-driven jets will be investigated in section 3.3.

The response of the NH polar vortex in $4CO_2+Solar$ is much weaker than $4CO_2+Sulfate$ (Figures 3c and 3d), indicating that it is dominated by the CO_2-driven component rather than by the solar dimming.

Table 2. Annual Frequency of Stratospheric Sudden Warming Events[a]

Name	Frequency
Control	0.68
$4CO_2$	0.63
$4CO_2$ + Sulfate	**0.016**
$4CO_2$ + Solar	**0.38**
$4CO_2$ + Titania	**0.031**

[a]Numbers in bold are significantly different from Control at the 95% level.

The polar vortex in the Southern Hemisphere (SH) is also intensified in the aerosol geoengineering simulations (Figures 3b and 3f). However, this does not result in SH polar stratospheric cooling because the SH polar vortex is already very strong and stable, which precludes significant dynamical feedbacks.

3.2. Polar Vortex

We now investigate the effects of the strongly enhanced stratospheric westerlies in the aerosol geoengineering simulations on the dynamics of the polar vortex. The frequency of stratospheric sudden warming events (SSWs) would be expected to decrease when the vortex is strengthened, assuming there is no change in vortex variability. Here SSWs are identified, using the method of *Charlton and Polvani* [2007], as reversals of the winter westerlies at 60°N, 10 hPa. Results are presented in Table 2. The $4CO_2$+*Sulfate* decreases the annual frequency of SSWs from 0.68 (44 SSWs in the 65 year simulation) to 0.016 (one SSW in 65 years). The $4CO_2$+*Solar* produces a relatively small decrease in SSW frequency, which is expected since the change in mean zonal wind is also small. There are two SSWs in 65 years in $4CO_2$+*Titania*, but at such a low sample size this is not significantly different from $4CO_2$+*Sulfate*.

The daily evolution of the polar vortex (as measured by the zonal mean zonal wind at 60°N, 10 hPa) is shown in Figure 4. In *Control* (Figure 4a), westerlies peak in early winter to midwinter at approximately 20 m s^{-1}. In $4CO_2$ (Figure 4b) the time-mean vortex winds are up to 5 m s^{-1} stronger between December and February. This small change in the strength of the polar vortex has little effect on the frequency of SSWs (Table 2). In the two aerosol geoengineering simulations the midwinter vortex winds are around 40 m s^{-1} stronger than *Control*, consistent with the significant reduction in SSW frequency. The very weakest winds in the 65 years of $4CO_2$+*Sulfate* are approximately equal to the mean winds of *Control*, illustrating how the strengthening of the polar vortex is readily apparent even in the presence of large variability. The $4CO_2$+*Solar* (Figure 4d) shows a small intensification of the polar vortex similar in magnitude to $4CO_2$. The magnitude of the variability changes little between the simulations. Therefore, warmings with respect to the mean state would occur with similar frequency in the *Control*, $4CO_2$, and geoengineering simulations, with similar implications for stratosphere-troposphere coupling. In a geoengineered world, stratospheric variability would still exert an influence on the troposphere in spite of the low SSW frequency.
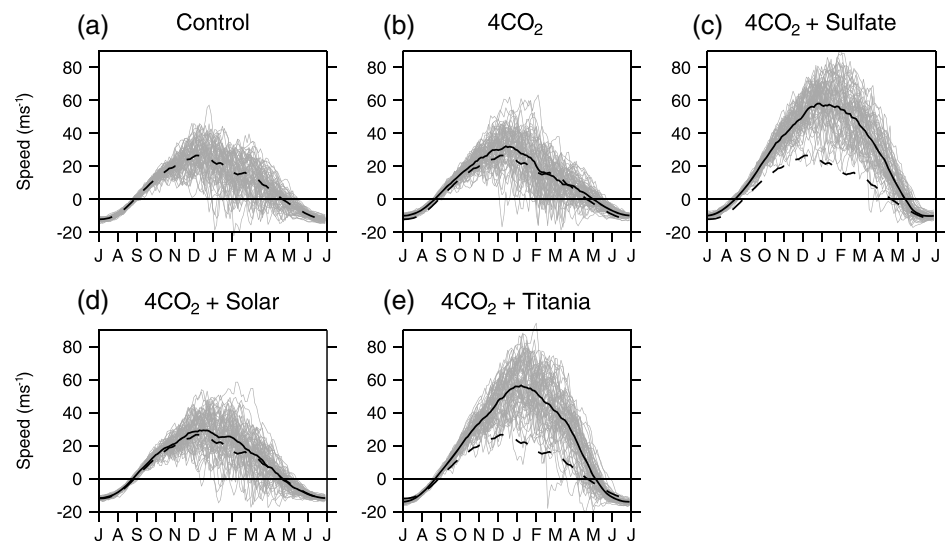

Figure 4. Daily evolution (starting in June of each year) of the zonal mean zonal wind speed at 60°N, 10 hPa. Each grey line shows the wind speed over 1 year. The mean of the *Control* simulation is shown by the dashed black lines. The means from the other simulations are shown by solid black lines.
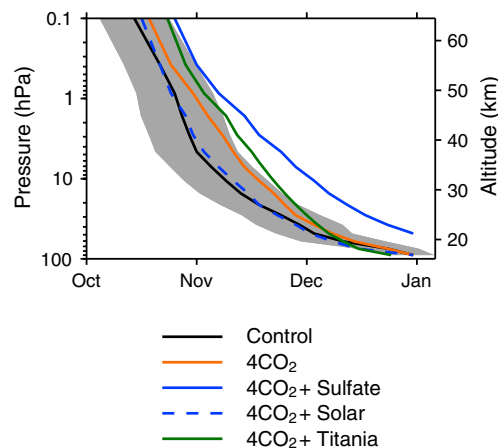
Figure 5. Mean date on which zonal mean zonal wind at 60°S becomes easterly. Tick marks denote the start of each month. Grey shading shows the interannual standard deviation for the *Control* simulation.

Since aerosol geoengineering ($4CO_2$+*Sulfate* and $4CO_2$+*Titania*) intensifies the polar vortex, we also expect a greater flux of wave activity into the stratosphere to be required for an SSW to occur. Following *Charlton and Polvani* [2007], we calculate the meridional heat flux anomaly at 100 hPa between 45°N and 75°N for the 20 days preceding an SSW as a proxy for wave activity entering the stratosphere. We must first verify that 45°N–75°N is an appropriate latitude range to use for all of the IGCM simulations. Figure S6 shows that the meridional heat flux averaged over the SSW season (November–April) peaks at approximately 60°N for all simulations, so a 30° interval centered on this latitude is reasonable.

In *Control* the mean heat flux preceding an SSW is between 3 and 17 K ms^{-1}, with a mean of approximately 8 K ms^{-1} (Figure S5). The intensification of the polar vortex in $4CO_2$+*Sulfate* means that a larger meridional heat flux is required to force an SSW event. The mean heat flux of approximately 15 K ms^{-1} is twice as high as *Control*. It must be noted, however, that the SSW heat flux for $4CO_2$+*Sulfate* is calculated from a single event, which means that no statistical representation of natural variability can be included. The $4CO_2$+*Solar* shows a slightly higher heat flux requirement, similar to $4CO_2$.

Changes in stratospheric winds (Figure 3) might be expected to influence the spatial scale of waves able to propagate in the stratosphere. Shorter waves (which have lower phase speeds) cannot propagate in faster background flows [*Andrews et al.*, 1987]. Therefore, we might expect a reduction in shorter waves in the stronger stratospheric westerlies of the $4CO_2$+*Sulfate* and $4CO_2$+*Titania* simulations. There is indeed some reduction at wave number 2 in the power spectral density of geopotential height at 60°N, 10 hPa in these simulations (Figure S8). However, $4CO_2$ shows an increase in power at wave number 2, despite having a modest increase in lower stratospheric westerlies. This may be caused by a change in the dominant wave number of tropospheric wave sources under greenhouse warming, as found by *Rind et al.* [1998].

We investigate the effect of geoengineering on the dynamics of the SH polar vortex, where SSWs are extremely rare, by comparing the final warming date in each of model simulations. Here the final warming is defined as the day on which the zonal mean zonal wind at 60°S becomes easterly. An intensified polar vortex has a later final warming date. The final warming date in the aerosol geoengineering simulations is later by about 4 weeks for sulfate and 2 weeks for titania (Figure 5). For $4CO_2$+*Sulfate* this change is greater than the interannual standard deviation of *Control* at all altitudes. The change is smaller for titania, which is likely a result of the warming of the SH polar winter stratosphere by absorption of solar radiation (Figure 2). There is no statistically significant change in the final warming date in the NH (not shown).

3.3. Eddy-Driven Jet Latitude

The latitude of the tropospheric eddy-driven jets is identified in the climate model simulations using the method of *Woollings et al.* [2010]. First, daily mean zonal wind is vertically averaged between 960 and 700 hPa. It is then zonally averaged over longitudes representing the main ocean basins: North Atlantic (0°W–60°W), North Pacific (135°E–235°E), and Southern Hemisphere (SH; all longitudes). Latitudes equatorward of 15° and poleward of 75° are removed. The jet latitude is identified as the location of the daily maximum of the filtered regional wind field. Probability density functions of jet latitude are obtained by smoothing histograms using the Gaussian kernel method of *Silverman* [1981]. Here we present the response of the jet latitude in a geoengineered climate in each season and each ocean basin and compare this to the response to a quadrupling of CO_2 alone.

Climate models generally simulate a poleward shift of the jets in response to increasing CO_2 concentrations [*Yin*, 2005; *Lorenz and DeWeaver*, 2007; *Lu et al.*, 2008]. In the North Atlantic, our $4CO_2$ simulation produces
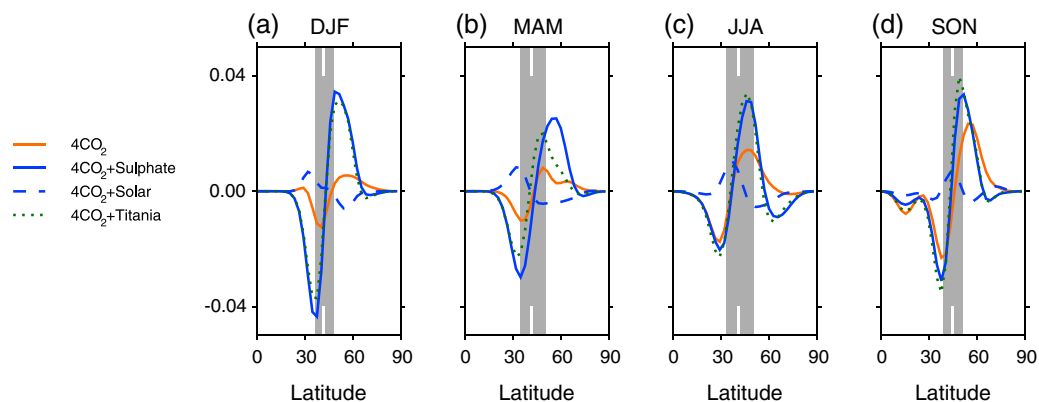
Figure 6. Changes in probability density function (units: probability per unit degree of latitude) of North Atlantic jet latitude in (a) DJF, (b) MAM, (c) JJA, and (d) SON. Grey shading shows the interquartile range of the *Control* simulation with the median marked with a white bar.

the most pronounced shift in the September-October-November (SON) season (Figure 6). In contrast, the aerosol geoengineering simulations produce the most pronounced poleward shift in DJF. This is consistent with the intensified Northern Hemisphere (NH) stratospheric polar vortex present in this season. The solar dimming simulation has little effect on the jet latitude. The magnitude of the jet shift in the aerosol geoengineering simulations exceeds the magnitude of the shift in the $4CO_2$ simulation in all seasons, not just seasons in which a polar vortex is present. Since there is no stratospheric polar vortex in summer, this suggests that the stratospheric influence is not the only cause of the simulated poleward jet shifts.

The North Pacific jet (Figure 7) behaves differently from the North Atlantic jet. Quadrupling CO_2 concentrations produces a small poleward shift in June-July-August (JJA) and SON and a reduction in latitudinal variability in DJF and (March-April-May) MAM. Aerosol geoengineering produces a poleward shift in DJF and MAM where there is none in $4CO_2$, indicating the influence of the stratospheric polar vortex on the North Pacific jet. The response to solar dimming is generally smaller than the responses to $4CO_2$ and the aerosol geoengineering simulations.

In the Southern Hemisphere (Figure 8), quadrupling CO_2 acts to shift the jet poleward in all seasons. Combining the quadrupling of CO_2 with aerosol geoengineering (as in the $4CO_2$ *Sulfate* and $4CO_2$+*Titania* simulations) produces a further poleward shift—again, aerosol geoengineering amplifies the effects of CO_2. The effect of geoengineering on the Southern Hemisphere jet latitude is greatest in SON and DJF. This is consistent with observations of stratosphere-troposphere coupling in the Southern Hemisphere
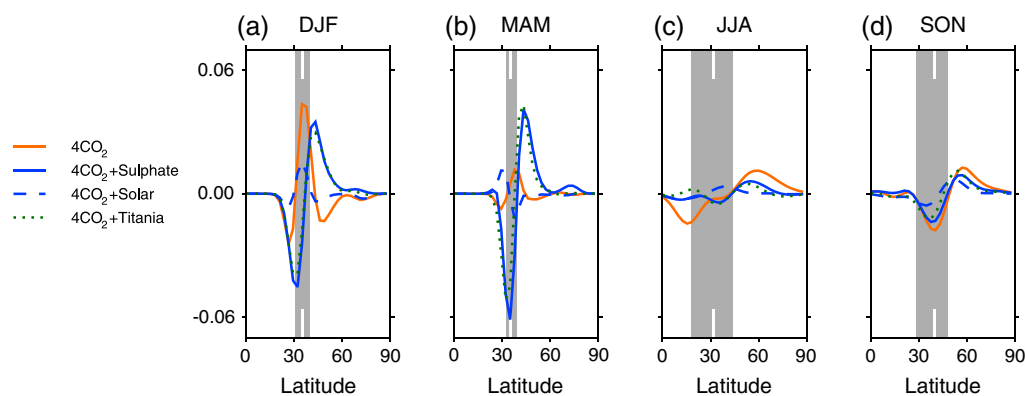

Figure 7. Changes in probability density function (units: probability per unit degree of latitude) of North Pacific jet latitude in (a) DJF, (b) MAM, (c) JJA, and (d) SON. Grey shading shows the interquartile range of the *Control* simulation with the median marked with a white bar.

Figure 8. Changes in probability density function (units: probability per unit degree of latitude) of Southern Hemisphere jet latitude in (a) DJF, (b) MAM, (c) JJA, and (d) SON. Grey shading shows the interquartile range of the *Control* simulation with the median marked with a white bar.
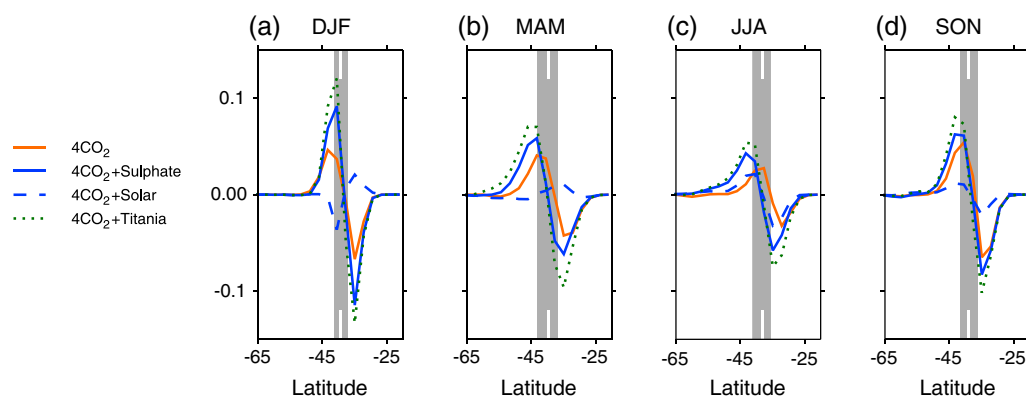
[*Thompson and Solomon*, 2002], where the period of greatest dynamical stratosphere-troposphere coupling occurs when the polar vortex is decaying. In the midwinter (JJA) period the SH polar vortex is too strong for planetary wave propagation, and dynamical coupling between the stratosphere and troposphere is not important.

The jet responses to aerosol geoengineering are not very sensitive to the type of aerosol used—sulfate and titania both produce poleward shifts since they both intensify the stratospheric polar vortex. Sulfate has a larger effect on the stratospheric meridional temperature gradient and consequently has a larger effect on the stratospheric polar vortex and the midlatitude jets. In contrast, solar dimming has a minimal effect on the stratospheric meridional temperature gradient and produces little change in vortex strength and in the midlatitude jets.

3.4. Brewer-Dobson Circulation

The strength of the Brewer-Dobson circulation (BDC) can be quantified by the upwelling mass flux at 70 hPa in the tropical pipe between the "turnaround latitudes" (the latitude at which the tropical upwelling changes to high-latitude downwelling). The $4CO_2$ simulation has a strengthened BDC (Figure 9). The $4CO_2+Solar$ shows a strengthening of tropical upwelling in all months, but the magnitude is less than that for $4CO_2$. The $4CO_2+Titania$ shows a comparable intensification to $4CO_2$, whereas $4CO_2+Sulfate$ has tropical upwelling which is stronger than $4CO_2$. The stronger BDC in $4CO_2+Sulfate$ than $4CO_2+Titania$ may explain the smaller tropical lower stratospheric warming seen in Figure 2, since an enhanced BDC increases adiabatic cooling in this region.
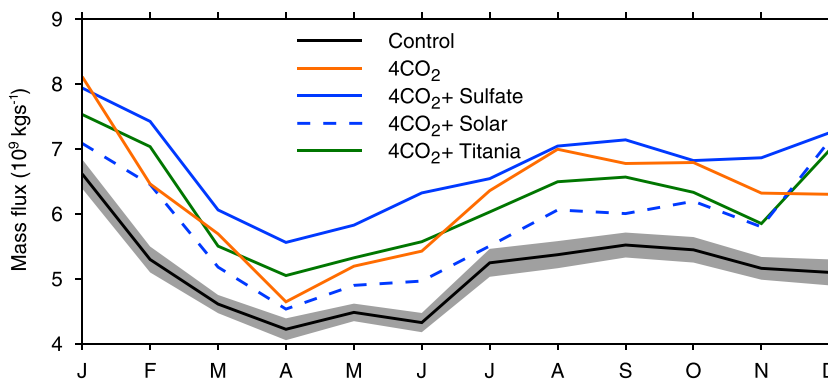

Figure 9. Monthly tropical upwelling mass flux at 70 hPa. The tropical upwelling is calculated at the mass flux between the "turnaround latitudes"—the latitude in each hemisphere where the tropical stratospheric upwelling transitions to high-latitude downwelling. The grey shading shows the 95% confidence interval for the annual *Control* climatology.
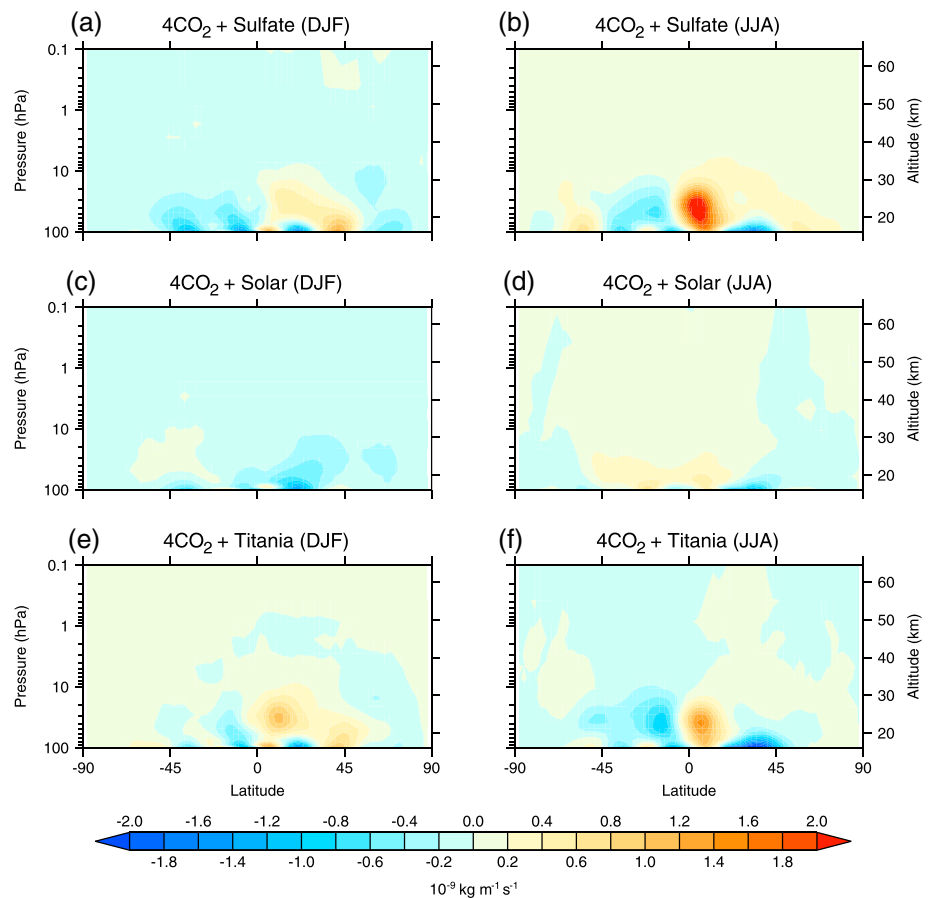
Figure 10. Response of the mean residual stream function ($kg\,m^{-1}\,s^{-1}$) compared to $4CO_2$. Positive values correspond to clockwise circulation.

Shepherd and McLandress [2010] suggested that the intensification of the BDC by CO_2 is a result of westerly anomalies on the upper flanks of the subtropical jets allowing greater wave penetration into the subtropical stratosphere. All three geoengineering simulations counteract these anomalies (Figure 3) because of the lack of tropical upper tropospheric warming. However, there are some lower stratospheric westerly anomalies which may act to increase the flux of wave activity into the stratosphere around the turnaround latitudes.

Changes in the spatial structure of the BDC can be presented using the transformed Eulerian mean residual stream function [*Andrews et al.*, 1987] (Figure 10). We present changes in the residual stream function relative to the $4CO_2$ simulation to emphasize that part of the response is due to the geoengineering aerosol rather than the increased CO_2 concentrations. If there is little response in Figure 10, this indicates that geoengineering has not counteracted the CO_2-driven intensification of the BDC. Corresponding responses relative to the *Control* simulation are shown in Figure S9. The $4CO_2$+*Sulfate* (Figures 10a and 10b) and $4CO_2$+*Titania* (Figures 10e and 10f) show some changes in stream function not present in $4CO_2$. The lower stratospheric part of the circulation is intensified, whereas the response above 10 hPa is similar to $4CO_2$. There is also an anomalous secondary circulation embedded into the BDC in the tropical lower stratosphere, most clearly visible in JJA (Figures 10b and 10f) but present in DJF as well. This anomalous circulation is a result of the strong tropical lower stratospheric heating from the aerosol layer. If the climate model used in this study allowed aerosol to be transported by the circulation, this stream function anomaly would produce heating-induced "self-lofting." Such effects have mostly been discussed in the context of black carbon aerosol [e.g., *Keith et al.*, 2010; *Kravitz et al.*, 2012], but here we see similar behavior even for comparatively small tropical lower stratospheric warming. In $4CO_2$+*Solar*, where there is no heating from stratospheric aerosol, this effect is not seen.

Importantly, however, Figure 10 shows little difference between $4CO_2$ and the aerosol geoengineering simulations above the aerosol layer. Where there is no radiative heating from the aerosol, the effect of CO_2 dominates and stratospheric aerosol geoengineering does not compensate for the strengthening of the BDC under CO_2-induced climate change.

4. Discussion

In this study we have shown that if it were possible to use stratospheric aerosols to counterbalance the surface warming from a quadrupling of CO_2, the stratospheric polar vortices would be strongly intensified relative to both present-day and high-CO_2 conditions, especially in the NH. SSW events would be nearly eliminated.

The large interannual variability in the stratospheric polar vortex means that long climate model simulations are required in order to identify statistically significant responses. Since SSWs become so rare in the aerosol geoengineering simulations, a detailed examination of the dynamics of SSW events in a geoengineered world was not possible in this study. However, our results show that the intensified polar vortex would reduce the spectral power of wave number 2 disturbances of the stratospheric geopotential height field. Since wave number 2 stratospheric disturbances tend to produce vortex-splitting SSWs [*Mitchell et al.*, 2013], there may be fewer vortex-splitting SSWs in a geoengineered world.

In the SH the polar vortex is too stable for the intensified winds associated with aerosol geoengineering to have any effect on its dynamics. However, we find a delay in SH polar vortex final warming date comparable in magnitude to those associated with anthropogenic ozone depletion [*Wilcox and Charlton-Perez*, 2013], which would also tend to drive the SH tropospheric jet poleward in the spring. The anthropogenic Antarctic ozone hole has been linked to changes in Southern Hemisphere surface climate, especially in summertime, extending as far equatorward as the subtropics [*Thompson et al.*, 2011]. These climate changes are primarily associated with shifts in the Southern Annular Mode (the primary mode of midlatitude variability in the Southern Hemisphere). These shifts have been linked to observed changes in surface temperature, such as the surface warming over southern Africa during the 1990s and 2000s [*Manatsa et al.*, 2013]. It is possible that stratospheric aerosol geoengineering could exert similar influences on the regional surface climate of the Southern Hemisphere.

In these model simulations the aerosol distribution was not allowed to interact with the meteorology, and ozone chemistry was not represented. This means that any dynamical feedbacks on the aerosol distribution or ozone concentration are not represented in these simulations. However, some inferences as to the consequences of the dynamical changes for ozone can be made.

Stratospheric aerosol geoengineering would not mitigate the strengthening of the BDC under increased CO_2 concentrations. The increased tropical upwelling in the BDC would act to decrease column ozone in the tropics, through import of low-ozone tropospheric air (in agreement with *Pitari et al.* [2014]), and increase it in the midlatitudes through increased downward transport of high-ozone upper stratospheric air. In simulations of future climate in which ozone-depleting substances are not present and the BDC is strengthened by anthropogenic greenhouse gas emissions, the ozone column in midlatitude to high-latitude experiences a superrecovery [*Li et al.*, 2009]. Since geoengineering would also intensify the BDC, a similar superrecovery might be expected in a geoengineered climate. Previous research [*Tilmes et al.*, 2009; *Pitari et al.*, 2014] has shown that stratospheric aerosol geoengineering would decrease polar stratospheric ozone. In this respect, interactive ozone coupling would be expected to enhance the stratospheric dynamical responses presented in this paper—the decreased polar stratospheric ozone would cool the polar stratosphere and intensify the polar vortex, further shifting the tropospheric jets poleward.

As mentioned in section 2, this study uses an aerosol median radius that is likely unrealistically small. Indeed, it is not at all clear whether the injection of sulfate into the stratosphere could achieve a strong enough radiative forcing to counterbalance the effects of a quadrupling of CO_2 concentrations, because as the mass of aerosol in the stratosphere increases, coagulation processes increase the size of the aerosols and decrease their lifetime in the stratosphere [*Heckendorn et al.*, 2009; *English et al.*, 2012]. Whether coagulation processes produce a similar effect for titania is unclear as relatively little research has been performed on the behavior of titania aerosol in the stratosphere. Our approach here has been to use idealized simulations with large forcings to aid interpretation of the climate model results. This approach is informative to the

extent that the response of climate system phenomena to forcings can be considered linear. However, a number of the phenomena considered in this study are known to be driven by highly nonlinear processes, notably stratospheric wave propagation and breaking in the polar vortex. It is therefore possible that the results presented in this paper are not easily applicable to scenarios with lower aerosol or greenhouse gas concentrations.

Ferraro et al. [2011] found that larger aerosol sizes tend to have a greater impact on the lower stratospheric meridional temperature gradient. Since we have used likely unrealistically small aerosols here, the impact on the stratospheric polar vortex strength for a given stratospheric aerosol loading might be greater than we calculate (again, this is assuming that large stratospheric aerosol loadings are achievable, which might not be the case, as discussed above).

There is also uncertainty in the aerosol spatial distribution. Modeling studies generally use similar injection strategies by injecting sulfur dioxide into the tropical stratosphere but produce different results as to the concentration of aerosol in the tropics relative to higher latitudes. For example, *Pitari et al.* [2014] show that aerosol optical depths strongly peaked in the tropics or almost uniform in latitude from different models. They attribute these differences to differences in meridional transport processes but also to aerosol size—the model with a more uniform distribution has prescribed aerosol size, whereas the model with a peaked distribution calculates the size interactively, simulating increasing aerosol growth and sedimentation in the tropical injection region and reducing the amount of aerosol available for transport to higher latitudes. Furthermore, *Benduhn and Lawrence* [2013] showed that the aerosol distribution is sensitive to the model's sedimentation scheme.

However, these uncertainties are unlikely to qualitatively affect our conclusions. This is because the effect of the aerosol on the meridional temperature gradient is not solely tied to the meridional gradient in aerosol concentration. *Ferraro et al.* [2011] showed that an anomalous meridional temperature gradient can be produced with a uniform aerosol distribution, with the different temperature responses at low and high latitudes determined by the local stratospheric temperatures (coldest in the tropics). The precise magnitude of the strengthening of the polar vortex will, however, be affected by the steepness and location of the anomalous meridional temperature gradient, so the results presented in this paper cannot be considered to be quantitatively accurate.

5. Conclusions

This study presents climate model simulations of the impact on the stratospheric dynamics of different solar radiation management geoengineering techniques. Space mirrors are represented by solar dimming, while stratospheric aerosol geoengineering is represented by prescribed layers of either sulfate or titania aerosol.

The polar vortices would intensify in response to tropical radiative heating by the aerosol, which shifts the tropospheric jets poleward in winter. This poleward shift would compound the poleward shift produced by increasing greenhouse gas concentrations. Such a poleward shift is not present in the solar dimming geoengineering experiment. Therefore, in terms of stratospheric dynamics, solar dimming experiments cannot be considered analogs for stratospheric aerosol geoengineering. Because the stratospheric polar vortices and tropospheric eddy-driven jets are intimately coupled, this also means that the tropospheric midlatitude dynamical response is different in solar dimming and stratospheric aerosol geoengineering experiments.

Stratospheric aerosol geoengineering does not counteract the strengthening of the BDC associated with increasing CO_2 concentrations. Indeed, in the case of sulfate the tropical lower stratospheric upwelling is further enhanced. This is at least partly because the aerosol radiative heating drives anomalous upwelling in the tropical lower stratosphere rather than being a simple intensification of the wave-driven stratospheric overturning.

These responses were seen in simulations of stratospheric aerosol geoengineering with both sulfate and titania aerosol. In general the magnitude of the dynamical response was stronger in the sulfate simulation, but substantial circulation changes remained in the titania simulation.

Thus, the representation of the stratosphere plays an important role in the response to stratospheric aerosol geoengineering. Since stratosphere-troposphere coupling plays a key role in determining the tropospheric

response to geoengineering, it is important that the stratospheric radiative and dynamical effects of the aerosol are represented as accurately as possible. However, even if the aerosol size, spatial distribution, and radiative effects were perfectly modeled, there would be uncertainty in the response due to differing model representations of stratosphere-troposphere coupling. Generally, climate models fail to capture the dynamical stratosphere-troposphere response to volcanic eruptions [*Stenchikov et al.*, 2006; *Driscoll et al.*, 2012; *Charlton-Perez et al.*, 2013].

The response will also be sensitive to the aerosol distribution and radiative properties since these determine the meridional temperature gradient, which affects the strength of the polar vortex. However, the physical mechanisms presented in this work are robust because the intensification of the polar vortex does not qualitatively depend on the aerosol layer properties (section 4). Our modeling framework did not include the interaction between the aerosol, stratospheric ozone, and stratospheric dynamics. Since ozone is very important for the radiation balance of the stratosphere, the response of ozone to stratospheric aerosol geoengineering will also have a dynamical effect. Climate models simulate a decrease in polar stratospheric ozone in response to stratospheric aerosol geoengineering [*Pitari et al.*, 2014], which would intensify the polar vortex and contribute further to the poleward shifts in the tropospheric jets found in this work.

References

Ammann, C. M., W. M. Washington, G. A. Meehl, L. Buja, and H. Teng (2010), Climate engineering through artificial enhancement of natural forcings: Magnitudes and implied consequences, *J. Geophys. Res.*, *115*, D22109, doi:10.1029/2009JD012878.

Andrews, D. G., J. R. Holton, and C. B. Leovy (1987), *Middle Atmosphere Dynamics*, Academic Press, San Diego, Calif.

Angel, R. (2006), Feasibility of cooling the Earth with a cloud of small spacecraft near the inner Lagrange point (L1), *Proc. Nat. Acad. Sci.*, *103*(46), 17,184–17,189, doi:10.1073/pnas.0608163103.

Aquila, V., C. I. Garfinkel, P. A. Newman, L. D. Oman, and D. W. Waugh (2014), Modifications of the Quasi-Biennial Oscillation by a geoengineering perturbation of the stratospheric aerosol layer, *Geophys. Res. Lett.*, *41*, 1738–1744, doi:10.1002/2013GL058818.

Bala, G., P. B. Duffy, and K. E. Taylor (2008), Impact of geoengineering schemes on the global hydrological cycle, *Proc. Nat. Acad. Sci.*, *105*(22), 7664–7669, doi:10.1073/pnas.0711648105.

Baldwin, M. P., and T. J. Dunkerton (1999), Propagation of the arctic oscillation from the stratosphere to the troposphere, *J. Geophys. Res.*, *104*(D24), 30,937–30,946, doi:10.1029/1999JD900445.

Baldwin, M. P., and T. J. Dunkerton (2001), Stratospheric harbingers of anomalous weather regimes, *Science*, *294*(5542), 581–584, doi:10.1126/science.1063315.

Bell, C. J., L. J. Gray, A. J. Charlton-Perez, M. M. Joshi, and A. A. Scaife (2009), Stratospheric communication of El Nino teleconnections to European winter, *J. Clim.*, *22*, 4083–4096, doi:10.1175/2009JCLI2717.1.

Bell, C. J., L. J. Gray, and J. Kettleborough (2010), Changes in Northern Hemisphere stratospheric variability under increased CO_2 concentrations, *Q. J. R. Meteorol. Soc.*, *136*, 1181–1190, doi:10.1002/qj.633.

Benduhn, F., and M. G. Lawrence (2013), An investigation of the role of sedimentation for stratospheric solar radiation management, *J. Geophys. Res. Atmos.*, *118*, 7905–7921, doi:10.1002/jgrd.50622.

Budyko, M. I. (1977), *Climatic Changes*, (Transl. Izmeniia Klimata, Gidrometeoizdat, Leningrad, 1974), AGU, Washington, D. C.

Butchart, N. (2014), The Brewer-Dobson circulation, *Rev. Geophys.*, *52*(2), 157–184, doi:10.1002/2013RG000448.

Butchart, N., et al. (2011), Multimodel climate and variability of the stratosphere, *J. Geophys. Res.*, *116*, D05102, doi:10.1029/2010JD014995.

Charlton, A. J., and L. M. Polvani (2007), A new look at stratospheric sudden warmings. Part I: Climatology and modeling benchmarks, *J. Clim.*, *20*(3), 449–469, doi:10.1175/JCLI3996.1.

Charlton-Perez, A. J., et al. (2013), On the lack of stratospheric dynamical variability in low-top versions of the CMIP5 models, *J. Geophys. Res. Atmos.*, *118*, 2494–2505, doi:10.1002/jgrd.50125.

Cnossen, I., H. Lu, C. J. Bell, L. J. Gray, and M. M. Joshi (2011), Solar signal propagation: The role of gravity waves and stratospheric sudden warmings, *J. Geophys. Res.*, *116*, D02118, doi:10.1029/2010JD014535.

Driscoll, S., A. Bozzo, L. J. Gray, A. Robock, and G. Stenchikov (2012), Coupled Model Intercomparison Project 5 (CMIP5) simulations of climate following volcanic eruptions, *J. Geophys. Res.*, *117*, D17105, doi:10.1029/2012JD017607.

Edwards, J. M., and A. Slingo (1996), Studies with a flexible new radiation code. I: Choosing a configuration for a large-scale model, *Q. J. R. Meteorol. Soc.*, *122*, 689–719, doi:10.1256/smsqj.53106.

English, J. M., O. B. Toon, and M. J. Mills (2012), Microphysical simulations of sulfur burdens from stratospheric sulfur geoengineering, *Atmos. Chem. Phys.*, *12*(10), 4775–4793, doi:10.5194/acp-12-4775-2012.

Ferraro, A. J. (2013), Atmospheric responses to geoengineering in the stratosphere, PhD thesis, Dept. of Meteorology, Univ. of Reading, Reading, Berkshire, U. K., doi:10.6084/m9.figshare.1014284.

Ferraro, A. J., E. J. Highwood, and A. J. Charlton-Perez (2011), Stratospheric heating by potential geoengineering aerosols, *Geophys. Res. Lett.*, *38*, L24706, doi:10.1029/2011GL049761.

Forster, P. M. F., M. Blackburn, R. Glover, and K. P. Shine (2000), An examination of climate sensitivity for idealised climate change experiments in an intermediate general circulation model, *Clim. Dyn.*, *16*, 833–849.

Garcia, R. R., and W. J. Randel (2008), Acceleration of the Brewer-Dobson circulation due to increases in greenhouse gases, *J. Atmos. Sci.*, *65*(8), 2731–2739, doi:10.1175/2008JAS2712.1.

Heckendorn, P., D. K. Weisenstein, S. Fueglistaler, B. P. Luo, E. V. Rozanov, M. Schraner, L. W. Thomason, and T. Peter (2009), The impact of geoengineering aerosols on stratospheric temperature and ozone, *Environ. Res. Lett.*, *4*, 045108, doi:10.1088/1748-9326/4/4/045108.

Irvine, P. J., A. Ridgwell, and D. J. Lunt (2010), Assessing the regional disparities in geoengineering impacts, *Geophys. Res. Lett.*, *37*, L18702, doi:10.1029/2010GL044447.

Jones, A., J. M. Haywood, and O. Boucher (2010), A comparison of the climate impacts of geoengineering by stratospheric SO2 injection and by brightening of marine stratocumulus cloud, *Atmos. Sci. Lett.*, *12*, 176–183, doi:10.1002/asl.291.

Keith, D. W., E. Parson, and M. G. Morgan (2010), Research on global Sun block needed now, *Nature*, *463*(7280), 426–427, doi:10.1038/463426a.

Knutti, R., and J. Sedláček (2012), Robustness and uncertainties in the new CMIP5 climate model projections, *Nat. Clim. Change*, *3*(4), 369–373, doi:10.1038/nclimate1716.

Kravitz, B., et al. (2013), Climate model response from the Geoengineering Model Intercomparison Project (GeoMIP), *J. Geophys. Res. Atmos.*, *118*, 8320–8332, doi:10.1002/jgrd.50646.

Kravitz, B. S., A. Robock, O. Boucher, H. Schmidt, K. E. Taylor, G. L. Stenchikov, and M. Schulz (2011), The Geoengineering Model Intercomparison Project (GeoMIP), *Atmos. Sci. Lett.*, *12*, 162–167, doi:10.1002/asl.316.

Kravitz, B. S., A. Robock, D. T. Shindell, and M. A. Miller (2012), Sensitivity of stratospheric geoengineering with black carbon to aerosol size and altitude of injection, *J. Geophys. Res.*, *117*, D09203, doi:10.1029/2011JD017341.

Lenton, T. M., and N. E. Vaughan (2009), The radiative forcing potential of different climate geoengineering options, *Atmos. Chem. Phys.*, *9*(15), 5539–5561, doi:10.5194/acp-9-5539-2009.

Li, D., and K. P. Shine (1995), A three dimensional ozone climatology for use in general circulation models, *UGAMP Internal Report 14*, Univ. of Reading, Reading, U. K.

Li, F., R. S. Stolarski, and P. A. Newman (2009), Stratospheric ozone in the post-CFC era, *Atmos. Chem. Phys.*, *9*(6), 2207–2213, doi:10.5194/acp-9-2207-2009.

Lorenz, D. J., and E. T. DeWeaver (2007), Tropopause height and zonal wind response to global warming in the IPCC scenario integrations, *J. Geophys. Res.*, *112*, D10119, doi:10.1029/2006JD008087.

Lu, J., G. Chen, and D. M. W. Frierson (2008), Response of the zonal mean atmospheric circulation to El Niño versus global warming, *J. Clim.*, *21*(22), 5835–5851, doi:10.1175/2008JCLI2200.1.

Manatsa, D., Y. Morioka, S. K. Behera, T. Yamagata, and C. H. Matarira (2013), Link between antarctic ozone depletion and summer warming over southern Africa, *Nat. Geosci.*, *6*(11), 934–939, doi:10.1038/ngeo1968.

Manzini, E., et al. (2014), Northern winter climate change: Assessment of uncertainty in CMIP5 projections related to stratosphere-troposphere coupling, *J. Geophys. Res. Atmos.*, *119*, 7979–7998, doi:10.1002/2013JD021403.

Mitchell, D. M., L. J. Gray, J. Anstey, M. P. Baldwin, and A. J. Charlton-Perez (2013), The influence of stratospheric vortex displacements and splits on surface climate, *J. Clim.*, *26*(8), 2668–2682, doi:10.1175/JCLI-D-12-00030.1.

Morcrette, J.-J. (1991), Radiation and cloud radiative properties in the European Centre for Medium Range Weather Forecasts Forecasting System, *J. Geophys. Res.*, *96*(D5), 9121–9132.

Nam, C., S. Bony, J.-L. Dufresne, and H. Chepfer (2012), The "too few, too bright" tropical low-cloud problem in CMIP5 models, *Geophys. Res. Lett.*, *39*, L21801, doi:10.1029/2012GL053421.

Niemeier, U., H. Schmidt, and C. Timmreck (2011), The dependency of geoengineered sulfate aerosol on the emission strategy, *Atmos. Sci. Lett.*, *12*(2), 189–194, doi:10.1002/asl.304.

Niemeier, U., H. Schmidt, K. Alterskjaer, and J. E. Kristjánsson (2013), Solar irradiance reduction via climate engineering—Impact of different techniques on the energy balance and the hydrological cycle, *J. Geophys. Res. Atmos.*, *118*, 11,905–11,917, doi:10.1002/2013JD020445.

Pierce, J. R., D. K. Weisenstein, P. Heckendorn, T. Peter, and D. W. Keith (2010), Efficient formation of stratospheric aerosol for climate engineering by emission of condensible vapor from aircraft, *Geophys. Res. Lett.*, *37*, L18805, doi:10.1029/2010GL043975.

Pitari, G., V. Aquila, B. Kravitz, A. Robock, S. Watanabe, I. Cionni, N. D. Luca, G. D. Genova, E. Mancini, and S. Tilmes (2014), Stratospheric ozone response to sulfate geoengineering: Results from the Geoengineering Model Intercomparison Project (GeoMIP), *J. Geophys. Res. Atmos.*, *119*, 2629–2653, doi:10.1002/2013JD020566.

Pope, F. D., P. Braesicke, R. G. Grainger, M. Kalberer, I. M. Watson, P. J. Davidson, and R. A. Cox (2012), Stratospheric aerosol particles and solar-radiation management, *Nat. Clim. Change*, *2*(10), 713–719, doi:10.1038/nclimate1528.

Ramachandran, S., V. Ramaswamy, G. L. Stenchikov, and A. Robock (2000), Radiative impact of the Mount Pinatubo volcanic eruption: Lower stratospheric response, *J. Geophys. Res.*, *105*(D19), 24,409–24,429.

Rasch, P. J., S. Tilmes, R. P. Turco, A. Robock, L. Oman, C.-C. Chen, G. L. Stenchikov, and R. R. Garcia (2008), An overview of geoengineering of climate using stratospheric sulphate aerosols, *Philos. Trans. R. Soc. A*, *366*(1882), 4007– 37, doi:10.1098/rsta.2008.0131.

Ribarsky, M. W. (1985), Titanium dioxide (TiO2) (Rutile), in *Handbook of Optical Constants of Solids*, edited by E. D. Palik, pp. 795–804, Academic, Burlington, doi:10.1016/B978-012544415-6.50042-X.

Ricke, K. L., M. G. Morgan, and M. R. Allen (2010), Regional climate response to solar-radiation management, *Nature Geosci.*, *3*(8), 537– 541, doi:10.1038/ngeo915.

Rind, D., D. Shindell, P. Longergan, and N. K. Balachandra (1998), Climate change and the middle atmosphere. Part III: The doubled CO$_2$ climate revisited, *J. Clim.*, *11*, 876– 894.

Robock, A., L. Oman, and G. L. Stenchikov (2008), Regional climate responses to geoengineering with tropical and Arctic SO$_2$ injections, *J. Geophys. Res.*, *113*, D16101, doi:10.1029/2008JD010050.

Robock, A., A. Marquardt, B. Kravitz, and G. Stenchikov (2009), Benefits, risks, and costs of stratospheric geoengineering, *Geophys. Res. Lett.*, *36*, L19703, doi:10.1029/2009GL039209.

Shepherd, T. G., and C. McLandress (2010), A robust mechanism for strengthening of the Brewer-Dobson circulation in response to climate change: Critical-layer control of subtropical wave breaking, *J. Atmos. Sci.*, *68*, 784–797, doi:10.1175/2010JAS3608.1.

Silverman, B. W. (1981), Using kernel density estimates to investigate multimodality, *J. R. Stat. Soc.*, *43*(1), 97–99.

Stenchikov, G. L., K. Hamilton, R. J. Stouffer, A. Robock, V. Ramaswamy, B. Santer, and H.-F. Graf (2006), Arctic oscillation response to volcanic eruptions in the IPCC AR4 climate models, *J. Geophys. Res.*, *111*, D07107, doi:10.1029/2005JD006286.

Thompson, D. W. J., and S. Solomon (2002), Interpretation of recent Southern Hemisphere climate change, *Science*, *296*(5569), 895–9, doi:10.1126/science.1069270.

Thompson, D. W. J., S. Solomon, P. J. Kushner, M. H. England, K. M. Grise, and D. J. Karoly (2011), Signatures of the antarctic ozone hole in Southern Hemisphere surface climate change, *Nat. Geosci.*, *4*(11), 741–749, doi:10.1038/ngeo1296.

Tilmes, S., R. Müller, and R. Salawitch (2008), The sensitivity of polar ozone depletion to proposed geoengineering schemes, *Science*, *320*(5880), 1201–4, doi:10.1126/science.1153966.

Tilmes, S., R. R. Garcia, D. E. Kinnison, A. Gettelman, and P. J. Rasch (2009), Impact of geoengineered aerosols on the troposphere and stratosphere, *J. Geophys. Res.*, *114*, D12305, doi:10.1029/2008JD011420.

Tilmes, S., M. J. Mills, U. Niemeier, H. Schmidt, A. Robock, B. Kravitz, J.-F. Lamarque, G. Pitari, and J. M. English (2014), A new Geoengineering Model Intercomparison Project (GeoMIP) experiment designed for climate and chemistry models, *Geosci. Model Dev. Discuss.*, *7*(4), 5447–5464, doi:10.5194/gmdd-7-5447-2014.

Uppala, S. M., et al. (2005), The ERA-40 re-analysis, *Q. J. R. Meteorol. Soc.*, *131*(612), 2961– 3012, doi:10.1256/qj.04.176.

Wilcox, L. J., and A. J. Charlton-Perez (2013), Final warming of the Southern Hemisphere polar vortex in high- and low-top CMIP5 models, *J. Geophys. Res. Atmos.*, *118*, 2535–2546, doi:10.1002/jgrd.50254.

World Meteorological Organisation (1986), *A Preliminary Cloudless Standard Atmosphere for Radiation Computation*, WCP-112, WMO/TD, No. 24.

Woollings, T., A. Hannachi, and B. Hoskins (2010), Variability of the North Atlantic eddy-driven jet stream, *Q. J. R. Meteorol. Soc.*, *136*(649), 856–868, doi:10.1002/qj.625.

Yin, J. H. (2005), A consistent poleward shift of the storm tracks in simulations of 21st century climate, *Geophys. Res. Lett.*, *32*, L18701, doi:10.1029/2005GL023684.